Journal of Materials Chemistry A

RSC Publishing

PAPER

View Article Online
View Journal | View Issue

Cite this: J. Mater. Chem. A, 2013, 1, 13101

Basic aluminum sulfate@graphene hydrogel composites: preparation and application for removal of fluoride†

Yunqiang Chen, Qingkun Zhang, Libin Chen, Hua Bai* and Lei Li*

Received 19th August 2013
Accepted 29th August 2013

DOI: 10.1039/c3ta13285d

www.rsc.org/MaterialsA

Porous composites based on basic aluminum sulfate and graphene hydrogel (BAS@GHG) were prepared *via* homogeneous precipitation of BAS in GHG, and used as adsorbents for fluoride removal from water. The BAS@GHG composites have a porous structure with a chemically converted graphene three dimensional network coated by a thin layer of amorphous BAS. These composites showed high adsorption capacities of up to 33.4 mg g^{-1} at equilibrium fluoride concentrations of 10.7 mg L^{-1} and temperatures of 298 K, higher than those of previously reported graphene and aluminum-based adsorbents. The adsorption kinetics and isotherm were analyzed by fitting experimental data with pseudo-first-order kinetics, the Weber–Morris model and Langmuir equations. The effects of temperature, pH value, and co-existing anions on the adsorption of fluoride were also investigated.

Introduction

Excess fluoride in drinking water has become a serious problem in many regions of the world.[1–3] Fluoride has both beneficial and detrimental effects on the human body depending on its concentration and the duration of exposure. Fluoride within the permissible limit of 0.5–1.5 mg L^{-1} is necessary for bone formation and the prevention of tooth decay, whereas excessive intake of fluoride has harmful effects on human health, causing dental fluorosis, musculo-skeletal fluorosis, osteoporosis, arthritis, and brittle bones.[4,5] Fluoride in drinking water may come from natural minerals or industrial discharge. Nowadays large numbers of fluorochemicals are used in many industries, such as ceramic production, semiconductor manufacturing, electroplating, coal fired power stations and aluminum smelters,[6] which usually discharge liquid waste containing fluoride with high concentrations. Fluoride can be removed from aqueous solutions by several methods, such as adsorption,[7,8] precipitation,[9] reverse osmosis,[10] ion exchange,[11] and electrolysis,[12] among which adsorption is the most widely used. Various materials, including hydroxyapatite,[13] aluminum hydroxides[14] and multi-walled carbon nanotubes,[15] have been employed as adsorbents for fluoride removal, and aluminum hydroxides are of great importance for industrial applications owing to their high affinity for fluoride. Fluoride is adsorbed on the positively charged surface of aluminum hydroxides through strong electrostatic force and a probable chemical reaction:[16]

$$Al(OH)_3 + xF^- \rightarrow Al(OH)_{3-x}F_x + xOH^-$$

However, the adsorption capacities of aluminum hydroxides are still not satisfactory, mainly due to the fact that for practical application the aluminum hydroxide powders usually have low specific surface areas. Therefore, to further improve the adsorption capacity of aluminum hydroxide based adsorbents, an efficient method is to increase their surface areas, for example, by introducing nanostructures.

Recently, graphene and its derivatives have demonstrated their capability as effective adsorbents for contaminant removal from water. Graphene possesses a unique two-dimensional (2D) structure composed of sp^2-hybridized carbon atoms and a large specific surface area (2630 m^2 g^{-1}),[17,18] and chemically converted graphene (CCG) has various oxygen-containing groups on its carbon skeleton. These characteristics render CCG an excellent adsorbent for dyes and metal ions.[19–22] However, although it was reported that CCG is able to adsorb fluoride from water,[23] the adsorption capacity is low, due to the weak interaction between CCG and fluoride. In this paper, combining the large specific surface area of graphene and high fluoride affinity of aluminum hydroxides, we design a new type of adsorbent by homogeneously depositing basic aluminum sulfate (BAS) onto porous graphene hydrogel (GHG). GHG is a three-dimensional (3D) CCG aggregate prepared by self-assembly during the reduction of graphene oxide (GO). The advantages of using GHG block but not CCG powder or dispersible CCG as a supporting matrix for BAS are that GHG blocks have large specific surface areas while being easy to

College of Materials, Xiamen University, Xiamen, 361005, P. R. China. E-mail: baihua@xmu.edu.cn; lilei@xmu.edu.cn

† Electronic supplementary information (ESI) available: EDAX spectra, dynamic rheological curve and BET adsorption/desorption curves of BAS@GHG composites. See DOI: 10.1039/c3ta13285d

remove from water after adsorption by decantation or filtration.[24] The BAS@GHG composites were prepared in two-steps: after GHG was synthesized by chemical reduction of GO, a homogeneous precipitation process was carried out to deposit BAS into the GHG. It was found that in the BAS@GHG composites a thin layer of BAS was coated evenly onto the CCG sheets in the porous GHG, an optimum structure for the adsorbent. The composites showed fast adsorption kinetics towards fluoride, and the adsorption capacity was measured to be 33.4 mg g^{-1} at an equilibrium concentration of 10.7 mg L^{-1}, higher than those of aluminum hydroxides and CCG.

Experimental

Chemicals and materials

Natural graphite powder was bought from Qingdao Huatai lubricant sealing S&T Co. Ltd (Qingdao, China). Aluminium sulfate, urea, sodium ascorbate, sodium chloride, sodium nitrate, sodium sulfate, sodium phosphate, sodium carbonate, trisodium citrate, acetic acid, concentrated nitric acid and sulfuric acid were purchased from Sinopharm Chemical Reagents Co. Ltd (Beijing, China). All the chemicals were used as received without further purification.

Preparation of BAS@GHG composites

GO was prepared from natural graphite powder with a modified Hummers method.[25,26] GHG was prepared by chemically reducing GO in a concentrated dispersion with sodium ascorbate.[27] Briefly, in a 15 mL glass vial 5 mL of GO aqueous dispersion (2 mg mL^{-1}) was loaded, in which 30 mg of sodium ascorbate was dissolved. Successively, the dispersion was heated at 90 °C for 1.5 h to produce the GHG. Soluble impurities in the GHG were then removed by dialysis.

To prepare BAS@GHG composites, the homogeneous precipitation of aluminum ions was carried out inside the GHG. To 5 mL of the $Al_2(SO_4)_3$ solution (0.5 M), 0.9 g of urea was added. After sonication for 30 min, the prepared GHGs were immersed in the homogeneous solution and kept there for 24 h to allow the solution to permeate into the GHGs. Then the solution containing GHGs was transferred into a 15 mL glass vial and heated at 95 °C for 45, 90, 135, 180, 225, 300 or 420 min. After cooling to room temperature, the obtained BAS@GHG composites were collected and dialyzed in pure water for 24 h to remove any soluble impurities. For comparison, pure BAS was prepared by homogeneous deposition for 180 min in the same solution without the presence of GHG, and purified by washing with pure water.

Batch adsorption experiments

In batch adsorption experiments, stock solution containing 2000 mg L^{-1} of fluoride ions was prepared by dissolving 442.1 mg of NaF in 100 mL of distilled water, and used to prepare other fluoride solutions. For each adsorption experiment, 100 mL of fluoride solution with different concentrations was mixed with 20 mg of lyophilized BAS@GHG composites or BAS powders in a 250 mL polypropylene flask. The flask was sealed and placed in a thermostatic water-bath. After stirring at 375 rpm for a certain period of time, 1 mL of the solution sample was taken for the concentration measurement. The fluoride concentrations were measured using a fluoride ion selective electrode (FISE, model PF-1) with a calomel electrode (model 217) as a reference.[28] The amount of adsorbed fluoride q_t (mg g^{-1}) at time t (h) was calculated using the following equation:

$$q_t = \frac{(C_0 - C_t)V}{m} \quad (1)$$

where C_0 and C_t are the concentrations of fluoride at 0 and t (mg L^{-1}), V is the volume of the solution (L), and m is the mass of the adsorbent (g).

To investigate the effect of pH on the fluoride adsorption capacity, the adsorption experiments were carried out at different pH in the range of 3.2–11.8. The pH of the solution was adjusted to a desired value using 0.1 M HNO_3 or 0.1 M NaOH solution. The influences of co-existing ions, including chloride, nitrate, sulfate, carbonate and phosphate, on the fluoride adsorption, were investigated by measuring the adsorption capacity in the presence of these ions. The initial concentration of fluoride was kept at 20 mg L^{-1} and those of co-existing ions were 200 mg L^{-1}.

Characterization

Scanning electron microscopy (SEM) images were recorded on a LEO 1530 scanning electron microscope operated at 20 kV. Transmission electron microscopy (TEM) observations were made with a JEM2100 transmission electron microscope at an acceleration voltage of 200 kV. To prepare the TEM samples, lyophilized samples were soaked in ethanol and sonicated for 5 min; afterwards a small drop of suspension was deposited onto a carbon-coated copper electron microscopy grid and dried at room temperature. The energy dispersion spectroscopy analysis was carried out on an energy dispersive spectrometer (ZNCA Energy TEM 100 X-ray energy spectrum) assembled on the JEM2100. X-ray diffraction (XRD) patterns were recorded using a D8 Advance (Bruker) X-ray diffractometer with Cu Kα radiation (λ = 1.5418 Å). Thermal gravimetric analysis (TGA) was performed on a Netzsch STA 409 EP thermal analyzer under an air atmosphere with a heating rate of 10 °C min^{-1} from room temperature to 750 °C. Specific surface areas were measured on a Micromeritics Tristar 3020 system. The measurement of aluminum concentrations was conducted using a MOLAAR M6 atomic absorption spectrophotometer (Thermo Scientific, USA).

Results and discussion

Preparation and characterization of BAS@GHG composites

BAS@GHG composites were synthesized following a two-step method. GHGs were firstly prepared by chemically reducing concentrated GO dispersion with ascorbic acid as a reductant.[27] During the reduction process, the GO sheets gradually lose hydrophilicity and form a 3D network.[29] Fig. 1a shows a photograph of as-prepared GHG as well as an SEM image of lyophilized GHG. A typical 3D network composed of 2D sheets

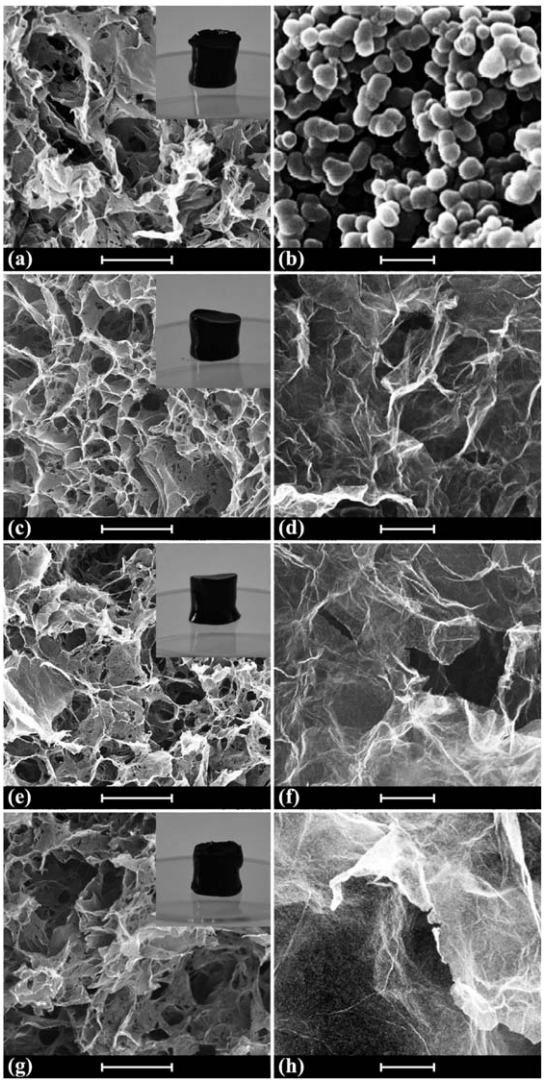

Fig. 1 SEM images of GHG (a), BAS (b) and BAS@GHG composites (c)–(h). Insets are the photographs of the corresponding samples. Scale bar: (a), (c), (e), (g) 10 μm, (b), (d), (f), (h) 500 nm.

can be found in the SEM image, and the pore sizes of the network are in the range of several to tens of micrometers.[30] In order to deposit BAS onto the 3D network of GHG, a homogeneous precipitation method was employed. Usually, aluminum hydroxides can be obtained as precipitates by alkalifying Al^{3+} solution, and the most convenient way is to directly mix Al^{3+} with alkali solutions. However, in our experiment, such a process is not applicable to deposit aluminum hydroxides inside the GHG, because the reaction is so fast that precipitate will form immediately when the two solutions contact. A homogeneous precipitation method can generate precipitation at a desired low rate, thus is suitable for the deposition of aluminum hydroxides inside the GHG. In the homogeneous precipitation process, aluminum sulfate was first mixed with urea solution and the GHGs were soaked in this solution. After the reactants diffused into the GHGs, the formation of aluminum hydroxides was triggered by heating the blend solution at 95 °C, when urea decomposed and released OH^-, precipitating aluminum ions in solution and inside the GHG. Aluminum sulfate was chosen as the source of Al^{3+}, because it can produce dense precipitate but other aluminum salts, such as aluminum chloride and aluminum nitride, will cause gelation during homogeneous precipitation.[31] We chose three composites (with deposition times of 90, 180 and 300 min, and denoted as BAS@GHG-1, -2 and -3, respectively) as examples for detailed study. As shown in the insets of Fig. 1, the shapes of the GHGs were preserved well after homogeneous deposition, and the composites showed good mechanical strength (Fig. S1 and S2†). The successful synthesis of aluminum hydroxides inside the GHGs is confirmed by energy dispersive X-ray analysis (EDAX), which shows that aluminum is found in all the composites. However, in these samples sulfur is also detected, indicating that sulfate ions co-precipitated into the precipitate, thus the precipitate is basic aluminum sulfate (or aluminum hydroxide containing sulfate).[31] The compositions of the resulting BSA precipitate were analyzed semi-quantitatively by EDAX. As listed in Table 1, the molar ratios of Al^{3+}/SO_4^{2-} are different for pure BAS and three composites. The BAS precipitate in BAS@GHG-2 and BAS@GHG-3 have similar compositions, with larger Al^{3+}/SO_4^{2-} values (4.8 and 4.7) than that in BAS@GHG-1 (2.4). This is because with longer deposition time more OH^- is produced, increasing the content of OH^- in the BAS precipitate. All three BAS@GHG composites have smaller Al^{3+}/SO_4^{2-} values than pure BAS (5.6), revealing that GHG participates in the formation of BAS and slightly alters its composition.

The morphologies of the BAS@GHG composites were investigated by electron microscopy. Fig. 1c, e and g are the SEM images of lyophilized BAS@GHG-1, -2 and -3, respectively. The morphologies of these composites resemble that of GHG (Fig. 1a), indicating that homogeneous precipitation did not damage the GHG framework. The BAS@GHG samples were uniform under SEM observation, and no particles were found in the samples, even in the magnified SEM images (Fig. 1d, f and h). Fig. 2 shows the TEM images of the GHG and BAS@GHG composites. The four TEM images are similar, showing thin 2D sheets with wrinkles, and still no obvious particles or aggregation are observed, although a large amount of aluminum was detected by EDAX on the sheets shown in Fig. 2b–d (Fig. S3†). Therefore, BAS must be distributed on the CCG sheets as an amorphous thin layer. This is interesting because BAS prepared with the homogeneous precipitation method without the presence of GHG consists of spherical particles, as shown in Fig. 1b.

Table 1 Al^{3+}/SO_4^{2-} ratio, BAS content and BET specific surface areas of GHG, BAS and BAS@GHG composites

	Al^{3+}/SO_4^{2-}	BAS content (%)	BET SSA/m^2 g^{-1}
GHG	—	0	246.2
BAS	5.6	100.0	1.9
BAS@GHG-1	2.4	26.5	144.2
BAS@GHG-2	4.8	33.7	128.9
BAS@GHG-3	4.7	40.9	40.4

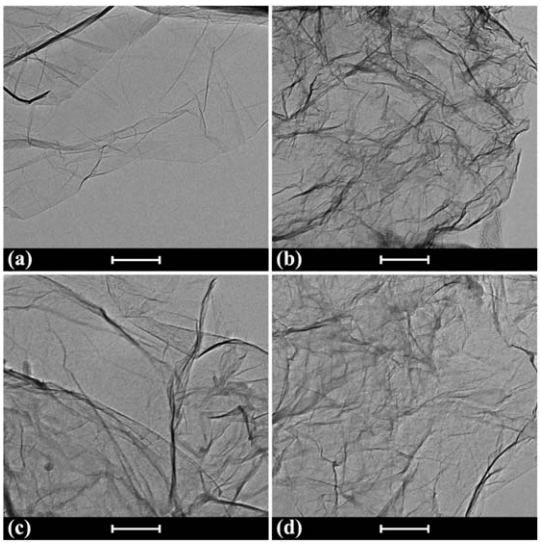

Fig. 2 TEM images of CCG (a), BAS@GHG-1 (b), BAS@GHG-2 (c) and BAS@GHG-3 (d). Scale bar: 200 nm.

These results reveal that GHG changes the nucleation and growth of the BAS during the homogeneous precipitation process. During the homogeneous precipitation, Al^{3+} or newly formed BAS may adsorb onto the CCG sheets due to the coordination of carboxyl and hydroxyl groups, and become nucleation sites, on which BAS continues to grow and cover the CCG sheets uniformly. Similar phenomena involving the crystallization of inorganic compounds being adjusted by graphene and its derivatives have also been observed in other systems.[32,33]

To further investigate the structure and composition of the BAS@GHG composites, thermogravimetric analysis (TGA) and X-ray diffraction (XRD) were performed. TGA was carried out to calculate the BAS content in the BAS@GHG composites. As shown in Fig. 3, a dramatic weight loss of GHG occurs at 380 to 600 °C, resulting in a low residual weight. This is assigned to the combustion and decomposition of the carbon skeleton. Pure BAS exhibits a weight loss from room temperature to 500 °C, due to the loss of adsorbed and coordinated water. The residual weight of BAS at 800 °C is 65.6%. All three BAS@GHG composites show similar thermal decomposition behavior, except for their residual weights being different. According to the residual weights at 800 °C, the BAS contents in BAS@GHG-1, -2 and -3 are calculated to be 26.5%, 33.7%, and 40.9%, respectively (Table 1). Therefore, the BAS content is well controlled by t_D. It is observed that the sharp weight loss of the BAS@GHG composites, corresponding to the decomposition of the GHG matrix, starts at ~500 °C, much higher than that of pure GHG (380 °C). This suggests that the thermal stability of GHG is improved by BAS. A possible reason is that the continuous BAS layer hinders the diffusion of oxygen and oxidation products, thus delays the oxidation reaction. The XRD patterns of the BAS, GHG and BAS@GHG composites are shown in Fig. 4. The XRD pattern of the BAS shows four broad peaks at locations of 8°, 20°, 40° and 65°, characteristic of amorphous BAS.[34] GHG has a broader peak centered at around 25°, corresponding to the interplanar distance of stacked CCG sheets.[30] In the XRD patterns of the BAS@GHG composites, no obvious peak related to BAS is found, except for the broad peak inherited from GHG. This result further confirms that the BAS phase in the composites is amorphous.

The specific surface area (SSA) is an important characteristic of adsorbents, and BET SSAs of pure the BAS, GHG and three BAS@GHG composites were measured by nitrogen adsorption at 77 K, as listed in Table 1. The N_2 adsorption/desorption isotherms (Fig. S4†) of these materials are characterized by type II isotherms with no hysteresis loops, indicating that no micropores or mesopores exist in these materials.[35] The SSA of pure BAS particles is only 1.9 $m^2\ g^{-1}$, while GHG shows a much higher SSA of 246.2 $m^2\ g^{-1}$, in agreement with the previously reported value.[36] After the deposition of BAS, the SSAs of the composites obviously decreased. In fact, since the BAS layer is compact, it cannot provide additional surface area for the composite. Meanwhile, the BAS layer significantly increases the weight of the sample. As a result, the SSAs of the BAS@GHG composites are smaller than that of the GHG. However, these SSA values are still much larger than that of pure BAS, which is beneficial for adsorption applications.

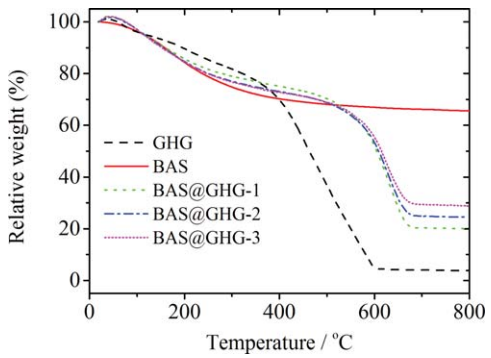

Fig. 3 Thermogravimetric analysis curves of BAS, GHG and BAS@GHG composites.

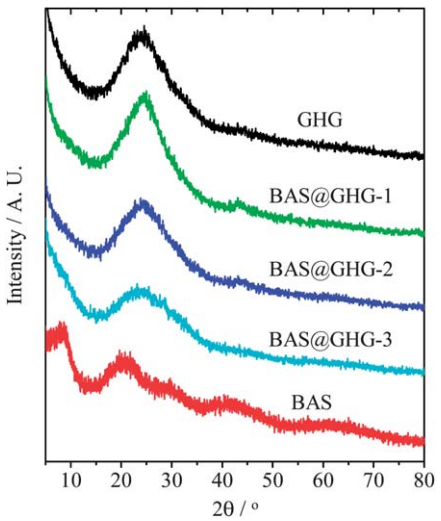

Fig. 4 X-ray diffraction patterns of BAS, GHG and BAS@GHG composites.

Adsorption kinetic studies

The BAS@GHG composites were tested as adsorbents for the removal of fluoride ions from water, and first their adsorption kinetics were investigated. The amount of fluoride adsorbed on the GHG, BAS and BAS@GHG composites (q_t) as a function of the contact time t, is shown in Fig. 5. As depicted in this figure, for all the adsorbents, the q_t values increase gradually with contact time and an equilibrium is reached in 120 min. The adsorption processes are analyzed by using reaction-based models, including pseudo-first-order and pseudo-second-order models. The pseudo-first-order rate equation can be represented as[37]

$$\frac{dq_t}{dt} = k_1(q_e - q_t) \quad (2)$$

where q_e is the adsorption capacity at equilibrium, and k_1 is the rate constant of the pseudo-first order adsorption reaction. The integrated pseudo-first-order rate equation under the boundary conditions $t = 0$, $q_t = 0$ is

$$q_t = q_e(1 - e^{-k_1 t}) \quad (3)$$

The pseudo-second-order model can be represented as:[38]

$$\frac{dq_t}{dt} = k_2(q_e - q_t)^2 \quad (4)$$

where q_e has the same meaning as above, and k_2 is the rate constant of the pseudo-second-order adsorption reaction. Its integrated form under the boundary conditions $t = 0$, $q_t = 0$ is:

$$q_t = \frac{k_2 q_e^2 t}{1 + k_2 q_e t} \quad (5)$$

The values of parameters k_1, k_2 and q_e are determined by nonlinear fitting of q_t against t according to eqn (3) and (5), and the validities of both kinetic models are assessed using the R^2 or χ^2 values. All these parameters and the coefficients obtained from the fitting are listed in Table 2. It was found that the experimental data fit better with the pseudo-first-order rate equation, because a smaller χ^2 and larger R^2 were obtained with this equation. The fitted pseudo-first-order kinetic curves are plotted in Fig. 5, and are consistent with the experimental data. The pseudo-first-order rate constant (k_1) can be used to compare the apparent adsorption rate on different adsorbents. k_1 values for the three BAS@GHG composites are in the range of 0.0265–0.0320 min^{-1}, comparable to that for BAS, which is 0.0325 min^{-1}. Therefore, the fluoride adsorption reactions on these adsorbents have similar apparent rates. As the pseudo-first-order rate constant includes the effect of the diffusion of fluoride, and the particle sizes of the BAS@GHG adsorbents (0.5–1 cm) are much larger than that of BAS (sub-micrometer), it is safe to conclude that the diffusion of fluoride in the porous BAS/GHG composites does not obviously lower the apparent adsorption rate. This enables us to use bulky adsorbents and remove them after adsorption by decantation.

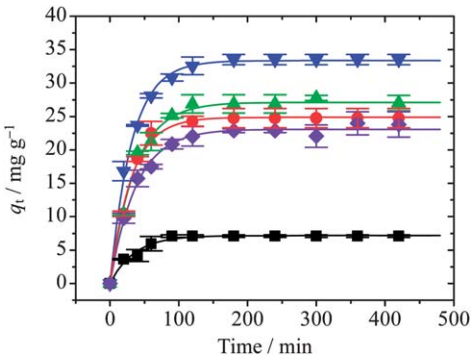

Fig. 5 Adsorption kinetic data of fluoride on GHG, BAS and BAS@GHG composites. ■: GHG, ●: BAS, ▲: BAS@GHG-1, ▼: BAS@GHG-2, ◆: BAS@GHG-3 (pH 7.2, adsorbent mass: 20 mg, temperature: 25 °C, initial fluoride concentration: 20 mg L^{-1}).

There are at least three steps in an adsorption process, which are external mass transfer (film diffusion) of the adsorbate, internal mass transfer (intraparticle diffusion) of the adsorbate, and mass action (adsorption reaction).[39] Either of the three steps can become the rate-limiting one, while the others remain in equilibrium. The BAS@GHG composites are porous and large in size, thus intraparticle diffusion may control the rate of the adsorption process. To obtain an insight into the adsorption mechanism, we further analyzed the adsorption kinetic data by using the Weber–Morris model:[40]

$$q_t = k_p t^{1/2} \quad (6)$$

where k_p is the intraparticle diffusion constant. If an adsorption process is controlled by the intraparticle diffusion of the adsorbate, its adsorption rate should obey eqn (6). As shown in Fig. 6 and Table 3, in the first 90 min of adsorption, a good linear relationship between q_t and $t^{1/2}$ is observed for all the adsorbents, indicating that intraparticle diffusion is the rate-limiting step. Moreover, since GHG and BAS@GHG have similar microcosmic structures, the varied k_p values of these adsorbents also reveal that the mass action steps in these adsorbents are quite different.

Adsorption capacities of different adsorbents

The q_e values of GHG, BAS and all seven different composites were measured and are listed in Table 4. It was found that at the initial stage of homogeneous deposition, q_e of the composite increases with deposition time (t_D), and then reaches a peak value (33.5 mg g^{-1}) at $t_D = 180$ min (BAS@GHG-2), then it begins to decrease gradually with a further increase of t_D. Again we take BAS@GHG-1, -2 and -3 as examples of the composites, together with GHG and BAS, to investigate the effect of t_D on the adsorption capacity. The adsorption capacity of GHG towards fluoride is only 7.2 mg g^{-1}, as listed in Table 4, despite its relatively large SSA. Considering the low nucleophilicity of fluoride ions in water, the adsorption mechanism of fluoride on CCG sheets should be physical adsorption, rather than a chemical reaction. However, there is no specific interaction between fluoride and CCG, while electrostatic repulsion further decreases the affinity between them.

Table 2 Fitted parameters for two types of reaction-based kinetic model

	Pseudo-first-order kinetics				Pseudo-second-order kinetics			
	k_1/min^{-1}	q_e/mg g^{-1}	R^2	Reduced χ^2	k_2/g mg^{-1} min^{-1}	q_e/mg g^{-1}	R^2	Reduced χ^2
GHG	0.0289	7.2	0.979	0.112	0.00571	7.8	0.959	0.217
BAS	0.0325	24.9	0.993	0.0550	0.00196	26.9	0.966	0.748
BAS@GHG-1	0.0278	27.1	0.991	0.776	0.00130	30.2	0.966	2.850
BAS@GHG-2	0.0320	33.4	0.992	0.245	0.00137	36.3	0.968	1.164
BAS@GHG-3	0.0265	23.1	0.993	0.407	0.00147	25.6	0.987	0.732

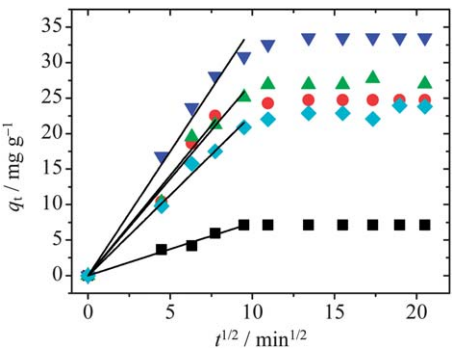

Fig. 6 Weber–Morris model plot of fluoride adsorption on GHG, BAS and BAS@GHG composites. ■: GHG, ●: BAS, ▲: BAS@GHG-1, ▼: BAS@GHG-2, ◆: BAS@GHG-3.

Table 3 Fitted parameters for the Weber–Morris model

	k_p/mg g^{-1} min$^{-1/2}$	R^2
GHG	0.74	0.996
BAS	2.82	0.992
BAS@GHG-1	2.73	0.992
BAS@GHG-2	3.52	0.995
BAS@GHG-3	2.27	0.990

Table 4 Fluoride adsorption capacities at equilibrium (q_e) of GHG, BAS and different BAS@GHG composites[a]

Deposition time/min	0[b]	45	90	135	180	225	300	420	∞[c]
q_e/mg g^{-1}	7.1	12.9	26.9	28.9	33.5	31.6	22.9	18.1	24.7

[a] Experimental conditions: pH 7.2, adsorbent mass 200 mg L^{-1}, temperature 298 K, initial fluoride concentration 20 mg L^{-1}. [b] Pure GHG. [c] Pure BAS.

Therefore the fluoride adsorption capacity on GHG is low. BAS particles, on the other hand, show high adsorption capacity of 24.9 mg g^{-1} towards fluoride. According to the literature, anion exchange may take place during the adsorption process: fluoride is believed to replace singly coordinated hydroxyl or water groups from the surface of aluminum hydroxides.[14] In this work, the sulfate ions in BAS may also take part in the anion exchange. Compared with hydroxide ions, sulfates have lower affinity for aluminum, therefore, in the thermodynamic sense, it is easier to replace them with fluoride than hydroxide ions. Consequently, the adsorption capacity of aluminum hydroxide is improved due to the existence of sulfate. However, BAS as an adsorbent is inconvenient for practical applications because it is difficult to remove from water after adsorption, due to its particle size being too small.

When BAS is supported on GHG, its adsorption capacity towards fluoride is dramatically increased. The q_e values for the three composites are 27.1, 33.4 and 23.1 mg g^{-1}, respectively. These values are larger than the reported maximum fluoride adsorption capacities of aluminum-based absorbents (12.57 mg g^{-1} on metallurgical grade alumina,[41] 3.26 mg g^{-1} on nano-scale aluminum oxide hydroxide,[42] 2.85 mg g^{-1} on manganese-oxide-coated alumina[43] and 15.4 mg g^{-1} on nano-alumina[44]). If we assume that the BAS layer does not decrease the adsorption capacity of the GHG matrix (7.2 mg g^{-1}), according to the BAS content measured by TGA, the adsorption capacities of BAS in the composites (q_{BAS}) are calculated to be 82.2, 84.9 and 46.1 mg g^{-1} for BAS@GHG-1, -2 and -3, respectively. In fact, the contribution of GHG to the total adsorption capacity must be less than 7.2 mg g^{-1} because its surface is covered by BAS. Therefore the adsorption capacities of the BAS in the three composites are larger than the above-mentioned values, within the limits of 102.2, 99.0 and 56.5 mg g^{-1} (neglecting the contribution of GHG). The improvement in adsorption capacity of BAS can be attributed to increase of their SSAs. All three of the BAS@GHG composites have much larger SSAs compared to BAS particles, therefore they possess more adsorption sites. Since the adsorption occurs mainly on the surface of the BAS, the thinner the BAS layer is, the higher the adsorption capacity (q_{BAS}) it can provide. The smaller q_e of BAS@GHG-1 is ascribed to a lower BAS content in this composite. In contrast the BAS layer of BAS@GHG-3 is too thick, resulting in a low SSA, as well as small q_{BAS} and q_e values. In the following sections, BAS@GHG-2 is used for further investigations, because it has the largest q_e and q_{BAS}. We also measured the aluminum content in the solution after adsorption, to evaluate the stability of the BAS@GHG adsorbents. After 7 h of adsorption by BAS@GHG-2, the aluminum content in the solution was 3.5 μg mL^{-1}. The aluminum species in the solution may come from formation of soluble Al–F complexes, and can be removed by the well-established methods in the water treatment industry.

Effect of temperature

Temperature is a crucial parameter for the adsorption process. To study the effect of temperature on the fluoride adsorption, the adsorption kinetic curves of fluoride on BAS@GHG-2 were measured at different temperatures, and fitted with a pseudo-first-order eqn (3), as depicted in Fig. 7. The fitted kinetic parameters at different temperatures are listed in Table 5, from which it is found that the q_e value increases with temperature, from 33.4 mg g^{-1} at 298 K to 40.0 and 46.5 mg g^{-1} at 313 and 328 K, respectively. Therefore increasing the temperature shifts the adsorption equilibrium to the right, showing that the fluoride adsorption process is endothermic.[44,45] However, the pseudo-first-order rate constant k_1 decreases as the temperature increases, from 0.032 min^{-1} at 298 K to 0.025 and 0.022 min^{-1} at 313 and 328 K, respectively, producing a negative apparent activation energy of −10.2 kJ mol^{-1} after fitting with the linear Arrhenius equation:

$$\ln k_1 = \ln A - \frac{E_a}{RT} \quad (7)$$

where A is the pre-exponential factor, E_a the apparent activation energy and R the gas constant. The negative apparent activation energy reveals that the adsorption is not an elementary reaction, whose activation energy is positive as for an endothermic reaction. Although the adsorption kinetics are first-order, the adsorption reaction mechanism may be complex. In fact, the BAS@GHG composites have heterogeneous surfaces with diverse adsorption sites, and for each type of adsorption site the reaction rate may be different. Also, these adsorption reactions may involve several elementary reactions. Therefore, the negative apparent activation energy is actually only a parameter indicating the phenomenon that the adsorption rate constant decreases with temperature. However, the total adsorption rate does increase with temperature owing to a larger q_e at higher temperature, thus for practical applications, a higher temperature is beneficial for fluoride removal.

Adsorption isotherm analysis

Equilibrium adsorption isotherms of fluoride on BAS@GHG-2 were measured using a batch procedure at pH 7.2 and 298 K.

Table 5 Kinetic parameters for fluoride adsorption on BAS@GHG-2 composites at different temperatures

T/K	k_1/min^{-1}	q_e/mg g^{-1}
298	0.032	33.4
313	0.025	40.0
328	0.022	46.5

Fig. 8 shows the obtained adsorption isotherms in an equilibrium fluoride concentration range of 2–32 mg L^{-1}. The adsorption capacity of fluoride at equilibrium (q_e) increases with the equilibrium concentration of fluoride (C_e) in the low concentration region, and tends to level off in the high concentration region. The isotherm models of Langmuir and Freundlich were used to analyze the experimental adsorption equilibrium data. The linear form of the Langmuir adsorption isotherm is expressed as follows:

$$\frac{1}{q_e} = \frac{1}{q_{max}} + \frac{1}{Kq_{max}}\frac{1}{C_e} \quad (8)$$

where q_{max} is the saturated adsorption capacity (mg g^{-1}), which gives the maximum adsorption capacity of the adsorbent, and K is the equilibrium constant. The values of K and q_{max} can be calculated by linear fitting of $1/q_e$ against $1/C_e$. The empirical Freundlich isotherm model can be expressed in a linear form as:

$$\log q_e = \log K_F + \frac{1}{n} \times \log C_e \quad (9)$$

where K_F and n are constants, whose values are calculated by the linear fitting of log q_e against log C_e. All the obtained parameters are listed in Table 6, from which it can be seen that the Langmuir isotherm model gives higher correlation coefficients R^2 = 0.997 than the Freundlich model (R^2 = 0.979). This indicates that the Langmuir model fits the experimental data well, and this is also confirmed by Fig. 8, in which both fitted isotherms are plotted and the Freundlich isotherm obviously deviates from the experimental data. According to the Langmuir model, the saturated adsorption capacity (q_{max}) of the

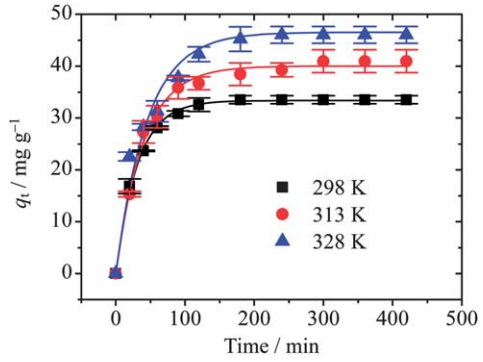

Fig. 7 Adsorption kinetic data of fluoride on BAS@GHG-2 composites at different temperatures (pH 7.2, adsorbent mass: 20 mg, temperature: 298 K, initial fluoride concentration: 20 mg L^{-1}).

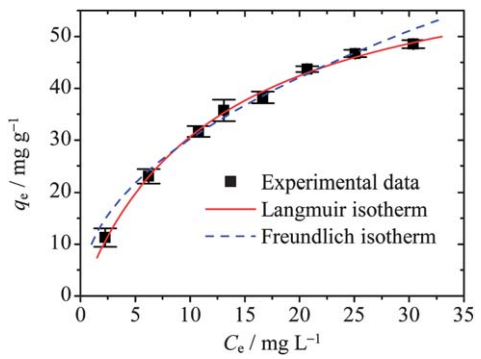

Fig. 8 Adsorption isotherm of fluoride on BAS@GHG-2 (volume of fluoride solution: 100 mL, adsorbent mass: 20 mg, temperature = 298 K, pH = 7.2).

Table 6 Isotherm parameters of fluoride adsorption on BAS@GHG-2 composites

Langmuir parameters			Freundlich parameters		
q_{max}/mg g^{-1}	K	R^2	K_F	n	R^2
68.9	0.0798	0.997	10	2.096	0.979

BAS@GHG-2 composite towards fluoride is 68.9 mg g^{-1} at 298 K.

Effect of pH

The solution pH can strongly influence the fluoride adsorption on BAS, because it effects not only the surface charge density of BAS but also the degree of ionization and speciation of fluoride. Fig. 9 shows the fluoride adsorption capacity of BAS@GHG-2 over a wide pH range from 3.2 to 11.8. The results show that q_e increases with pH in the acidic range and reaches a maximum value of 35 mg g^{-1} at pH = 7.2. Further increasing the pH causes q_e to decrease. In acidic solution fluoride ions will be protonated partially, forming hydrofluoric acid, thus the amount of fluoride adsorption on BAS@GHG-2 at acidic pH is less than that at neutral pH. Also, in acidic solution BAS tends to dissolve through the formation of AlF complexes,[46,47] which is undesirable for adsorption applications. The decrease of q_e in alkaline pH can be attributed to the competition for surface adsorption sites between the negative hydroxide ions and fluoride ions.[48] Besides, BAS may be converted to soluble *meta*-aluminate ions and dissolve in alkaline solution. Therefore, according to the data shown in Fig. 9, the optimum pH range for the BAS@GHG-2 adsorbent is 7–8.

Effects of co-existing anions

Contaminated water contains a variety of anions such as sulfate, phosphate, chloride and nitrate; these anions may compete with fluoride ions for the adsorption sites on the surface of the adsorbents. Therefore, it is necessary to study the influence of co-existing anions on fluoride adsorption. The effects of sulfate, nitrate, chloride, carbonate and phosphate on fluoride removal were investigated by measuring the fluoride adsorption capacity of BAS@GHG-2 in the presence of these anions (Fig. 10). The concentration of each co-existing anion was set as 200 mg L^{-1}, while the initial concentration of fluoride was 20 mg L^{-1}. It can be observed in Fig. 10 that Cl^-, NO_3^- and SO_4^{2-} ions exert little influence on the adsorption capacity of BAS@GHG-2 towards fluoride, whereas co-existing CO_3^{2-} and PO_4^{3-} ions have a negative effect on the fluoride adsorption. To explain these results, the change of the solution pH caused by the co-existing anions is taken into account. The pH values of the mixed solution of fluoride with Cl^-, NO_3^-, SO_4^{2-}, CO_3^{2-} and PO_4^{3-} were measured to be 7.08, 7.15, 7.22, 10.56 and 11.25, respectively, while the pH of the fluoride solution without the above co-existing ions was 7.24. Therefore, CO_3^{2-} and PO_4^{3-} significantly increase the pH of the fluoride solution through hydrolysis, and consequently suppress the adsorption of fluoride, as discussed in the above section. These results also reveal that Cl^-, NO_3^- and SO_4^{2-} do not compete with fluoride ions for the adsorption sites on BAS@GHG-2. However, such competition may occur in the cases of CO_3^{2-} and PO_4^{3-}, as reported for other Al-based adsorbents.[49–52]

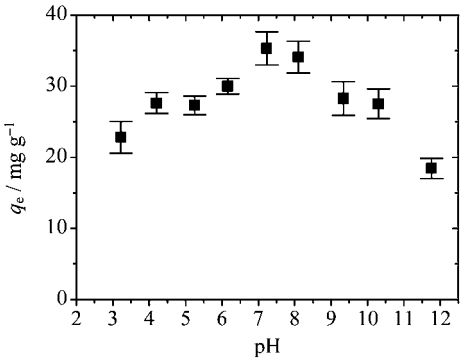

Fig. 9 Effect of initial pH on fluoride adsorption on BAS@GHG-2 composites (adsorbent mass: 20 mg, temperature: 298 K, initial fluoride concentration: 20 mg L^{-1}).

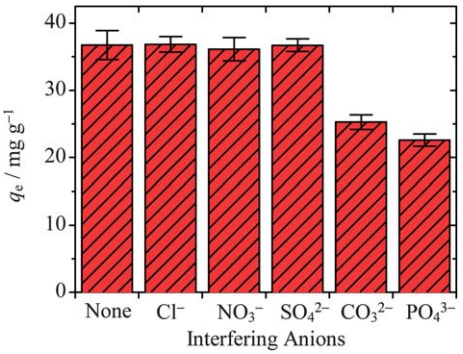

Fig. 10 Effects of co-existing anions on the fluoride adsorption on BAS@GHG-2 (concentration of co-ions: 200 mg L^{-1}, initial concentration of fluoride: 20 mg L^{-1}, adsorbent mass: 20 mg, temperature: 298 K).

Conclusions

In this paper, we prepared novel composites of BAS@GHG by depositing BAS in GHG using a homogeneous precipitation method. Thanks to the slow precipitation rate of homogeneous precipitation, BAS can be deposited uniformly onto the GHG network. SEM, TEM and XRD results reveal that BAS on the GHG matrix is a thin amorphous layer, and its content in the composites can be controlled by controlling the precipitation time. The BAS@GHG composites were then used as adsorbents for fluoride removal from water. Owing to the large size, the composite adsorbents are easy to remove from water, indicating good practicality for applications. The highest adsorption capacity of the BAS@GHG composites towards fluoride was found to be 33.4 mg g^{-1} at pH = 7.2 and 298 K, higher than those of BAS and CCG. In the composites, BAS is believed to result in the high fluoride adsorption capacity, due

to a ligand exchange mechanism between the hydroxide ions and fluoride ions, while GHG acts as a porous matrix which can provide a large surface area and facilitate the diffusion of the adsorbate. Kinetic and thermodynamic studies reveal that the fluoride adsorption on BAS@GHG can be described by a pseudo-first-order model, and the adsorption isotherm can be fitted well with the Langmuir equation. Moreover, the effect of pH and co-existing anions on the fluoride adsorption were investigated to further evaluate the performance of the BAS@GHG adsorbents. All these results demonstrate that the BAS@GHG composites are effective adsorbents for fluoride removal. We also believe that our preparation method involving homogeneous precipitation can be used to prepare other functional GHG composites.

Acknowledgements

The authors thank the National Natural Science Foundation of China (21104041) for financial support.

Notes and references

1 A. Bhatnagar, E. Kumar and M. Sillanpää, *Chem. Eng. J.*, 2011, **171**, 811.
2 M. Mohapatra, S. Anand, B. Mishra, D. E. Giles and P. Singh, *J. Environ. Manage.*, 2009, **91**, 67.
3 R. Maheshwari, *J. Hazard. Mater.*, 2006, **137**, 456.
4 J. Zhu, H. Zhao and J. Ni, *Sep. Purif. Technol.*, 2007, **56**, 184.
5 H. Wang, J. Chen, Y. Cai, J. Ji, L. Liu and H. H. Teng, *Appl. Clay Sci.*, 2007, **35**, 59.
6 E. Kumar, A. Bhatnagar, M. Ji, W. Jung, S. H. Lee, S. J. Kim, G. Lee, H. Song, J. Y. Choi, J. S. Yang and B. H. Jeon, *Water Res.*, 2009, **43**, 490.
7 X. Wu, Y. Zhang, X. Dou and M. Yang, *Chemosphere*, 2007, **69**, 1758.
8 S. S. Tripathy and A. M. Raichur, *J. Hazard. Mater.*, 2008, **153**, 1043.
9 H. Mjengera and G. Mkongo, *Phys. Chem. Earth*, 2003, **28**, 1097.
10 P. Sehn, *Desalination*, 2008, **223**, 73.
11 C. Sairam Sundaram and S. Meenakshi, *J. Colloid Interface Sci.*, 2009, **333**, 58.
12 Z. Amor, B. Bariou, N. Mameri, M. Taky, S. Nicolas and A. Elmidaoui, *Desalination*, 2001, **133**, 215.
13 Y. Wang, N. Chen, W. Wei, J. Cui and Z. Wei, *Desalination*, 2011, **276**, 161.
14 R. Liu, W. Gong, H. Lan, Y. Gao, H. Liu and J. Qu, *Chem. Eng. J.*, 2011, **175**, 144.
15 M. Ansari, M. Kazemipour, M. Dehghani and M. Kazemipour, *J. Fluorine Chem.*, 2011, **132**, 516.
16 X. Zhao, J. Wang, F. Wu, T. Wang, Y. Cai, Y. Shi and G. Jiang, *J. Hazard. Mater.*, 2010, **173**, 102.
17 S. Park and R. S. Ruoff, *Nat. Nanotechnol.*, 2009, **4**, 217.
18 N. Behabtu, J. R. Lomeda, M. J. Green, A. L. Higginbotham, A. Sinitskii, D. V. Kosynkin, D. Tsentalovich, A. N. G. Parra-Vasquez, J. Schmidt, E. Kesselman, Y. Cohen, Y. Talmon, J. M. Tour and M. Pasquali, *Nat. Nanotechnol.*, 2010, **5**, 406.
19 H. L. Ma, Y. W. Zhang, Q. H. Hu, D. Yan, Z. Z. Yu and M. L. Zhai, *J. Mater. Chem.*, 2012, **22**, 5914.
20 H. Jabeen, V. Chandra, S. Jung, J. W. Lee, K. S. Kim and S. Bin Kim, *Nanoscale*, 2011, **3**, 3583.
21 G. Xie, P. Xi, H. Liu, F. Chen, L. Huang, Y. Shi, F. Hou, Z. Zeng, C. Shao and J. Wang, *J. Mater. Chem.*, 2012, **22**, 1033.
22 Z. Geng, Y. Lin, X. Yu, Q. Shen, L. Ma, Z. Li, N. Pan and X. Wang, *J. Mater. Chem.*, 2012, **22**, 3527.
23 Y. Li, P. Zhang, Q. Du, X. Peng, T. Liu, Z. Wang, Y. Xia, W. Zhang, K. Wang and H. Zhu, *J. Colloid Interface Sci.*, 2011, **363**, 348.
24 Y. Chen, L. Chen, H. Bai and L. Li, *J. Mater. Chem. A*, 2013, **1**, 1992.
25 W. S. Hummers and R. E. Offeman, *J. Am. Chem. Soc.*, 1958, **80**, 1339.
26 Y. X. Xu, H. Bai, G. W. Lu, C. Li and G. Q. Shi, *J. Am. Chem. Soc.*, 2008, **130**, 5856.
27 K. Sheng, Y. Xu, C. Li and G. Shi, *New Carbon Mater.*, 2011, **26**, 9.
28 H. Wang, J. Chen, Y. Cai, J. Ji, L. Liu and H. H. Teng, *Appl. Clay Sci.*, 2007, **35**, 59.
29 C. Li and G. Q. Shi, *Nanoscale*, 2012, **4**, 5549.
30 Y. X. Xu, K. X. Sheng, C. Li and G. Q. Shi, *ACS Nano*, 2010, **4**, 4324.
31 L. Gordon, M. L. Salutsky and H. H. Willard, *Precipitation from homogeneous solution*, Wiley, New York, 1959.
32 X. Huang, S. Li, Y. Huang, S. Wu, X. Zhou, S. Li, C. L. Gan, F. Boey, C. A. Mirkin and H. Zhang, *Nat. Commun.*, 2011, **2**, 292.
33 X. L. Wang, H. Bai, Y. Y. Jia, L. J. Zhi, L. T. Qu, Y. X. Xu, C. Li and G. Q. Shi, *RSC Adv.*, 2012, **2**, 2154.
34 K. Fukushi, K. Tsukimura and H. Yamada, *Acta Geol. Sin.*, 2006, **80**, 206.
35 K. Sing, D. Everett, R. Haul, L. Moscou, R. Pierotti, J. Rouquerol and T. Siemieniewska, *Pure Appl. Chem.*, 1982, **54**, 2201.
36 L. Zhang and G. Q. Shi, *J. Phys. Chem. C*, 2011, **115**, 17206.
37 S. Lagergren and B. K. Svenska, *Vetenskapsakad. Handl.*, 1898, **24**, 1.
38 Y. S. Ho and G. McKay, *Process Biochem.*, 1999, **34**, 451.
39 G. E. Boyd, A. W. Adamson and J. R. Myers, *J. Am. Chem. Soc.*, 1947, **69**, 2836.
40 W. J. Weber and J. C. Morris, *J. Sanit. Eng. Div., Am. Soc. Civ. Eng.*, 1963, **83**, 31.
41 L. Pietrelli, *Ann. Chim.*, 2005, **95**, 303.
42 S. Wang, Y. Ma, Y. Shi and W. Gong, *J. Chem. Technol. Biotechnol.*, 2009, **84**, 1043.
43 S. M. Maliyekkal, A. K. Sharma and L. Philip, *Water Res.*, 2006, **40**, 3497.
44 E. Kumar, A. Bhatnagar, U. Kumar and M. Sillanpää, *J. Hazard. Mater.*, 2011, **186**, 1042.
45 X. Zhao, J. Wang, F. Wu, T. Wang, Y. Cai, Y. Shi and G. Jiang, *J. Hazard. Mater.*, 2010, **173**, 102.
46 H. Farrah, J. Slavek and W. Pickering, *Aust. J. Soil Res.*, 1987, **25**, 55.

47 A. López Valdivieso, J. Reyes Bahena, S. Song and R. Herrera Urbina, *J. Colloid Interface Sci.*, 2006, **298**, 1.
48 N. Viswanathan, C. S. Sundaram and S. Meenakshi, *Colloids Surf., B*, 2009, **68**, 48.
49 M. Mahramanlioglu, I. Kizilcikli and I. O. Bicer, *J. Fluorine Chem.*, 2002, **115**, 41.
50 M. G. Sujana, R. S. Thakur and S. B. Rao, *J. Colloid Interface Sci.*, 1998, **206**, 94.
51 S. K. Swain, T. Patnaik, V. K. Singh, U. Jha, R. K. Patel and R. K. Dey, *Chem. Eng. J.*, 2011, **171**, 1218.
52 S. P. Kamble, S. Jagtap, N. K. Labhsetwar, D. Thakare, S. Godfrey, S. Devotta and S. S. Rayalu, *Chem. Eng. J.*, 2007, **129**, 173.